Supporting Information for:

Microfluidic encapsulation of hydrophobic antifouling biocides in calcium-alginate hydrogels for controllable release

Yingzhe Liu[†] and Takasi Nisisako*[‡]

† Department of Mechanical Engineering, School of Engineering, Tokyo Institute of Technology, Tokyo, 152-8552 Japan

‡ Institute of Innovative Research, Tokyo Institute of Technology, R2-9, Nagatsuta-cho, Midori-ku, Yokohama, Kanagawa, 226-8503 Japan

*To whom correspondence should be addressed: nisisako.t.aa@m.titech.ac.jp

Supporting information includes:

Figure S-1. Introduction of antifouling biocides into paint formulation.

Figure S-2. Antifouling mechanism of Irgarol on aquatic plant species.

Figure S-3. Scanning electron microscopy (SEM) images of the cross-section of the Ca-alginate hydrogel particles.

Figure S-4. ATR-FTIR spectra of sodium alginate (Na-alginate) powder, synthesized Ca-alginate particles, Ca-alginate particles containing Irgarol, and Irgarol powder.

Figure S-5. High speed photomicrographs showing the break-off of a Na-alginate droplet containing both the drug and cellulose fibers.

Figure S-6. A photograph from the side showing the particles deformation measurement.

Figure S-7. A SEM image of the cellulose fibers.

Figure S-8. Schematic illustration of the UV-Vis measurement process.

Figure S-9. Measurement of UV-Vis absorbance spectra of Irgarol (Sample 1) at different dilution ratios.

Figure S-10. Relationship between the UV-Vis absorbance and the drug concentration.
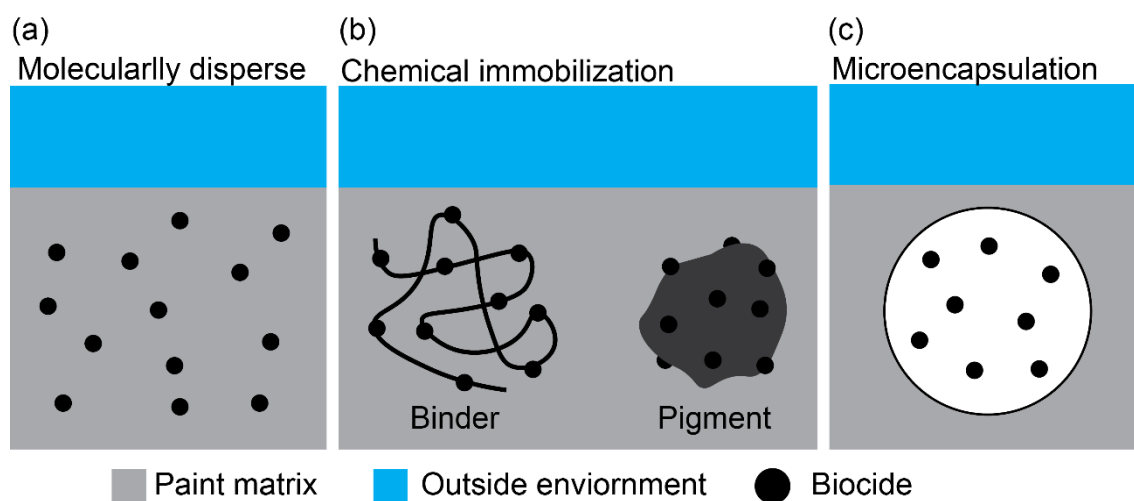
Table S-1. Sizes and size distributions of microcapsules for biocides encapsulation in literature.

Table S-2. Contents of the disperse phase used in the experiment.
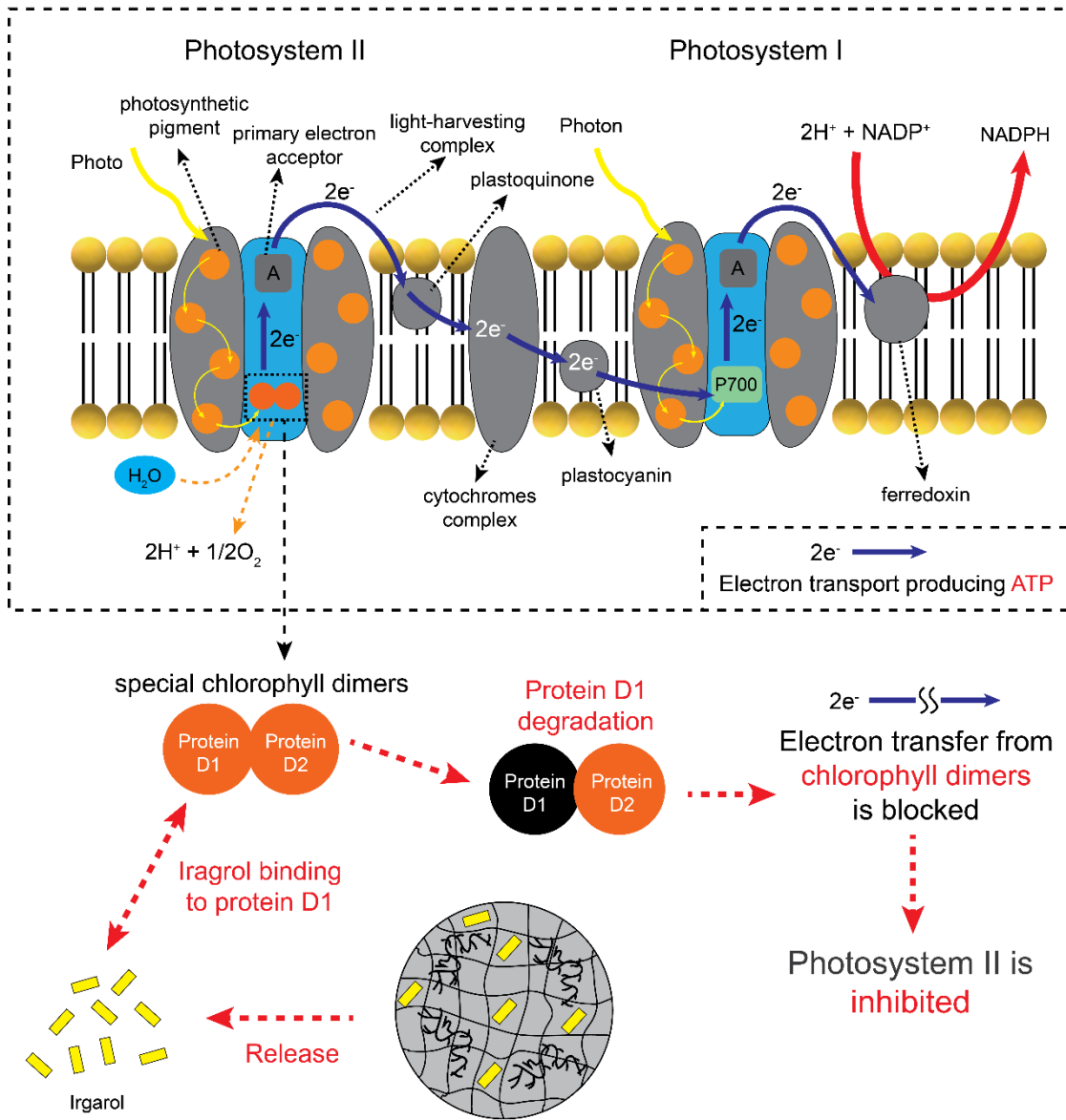
Table S-3. The details of the five samples.

Table S-4. Results of the linear fitting.

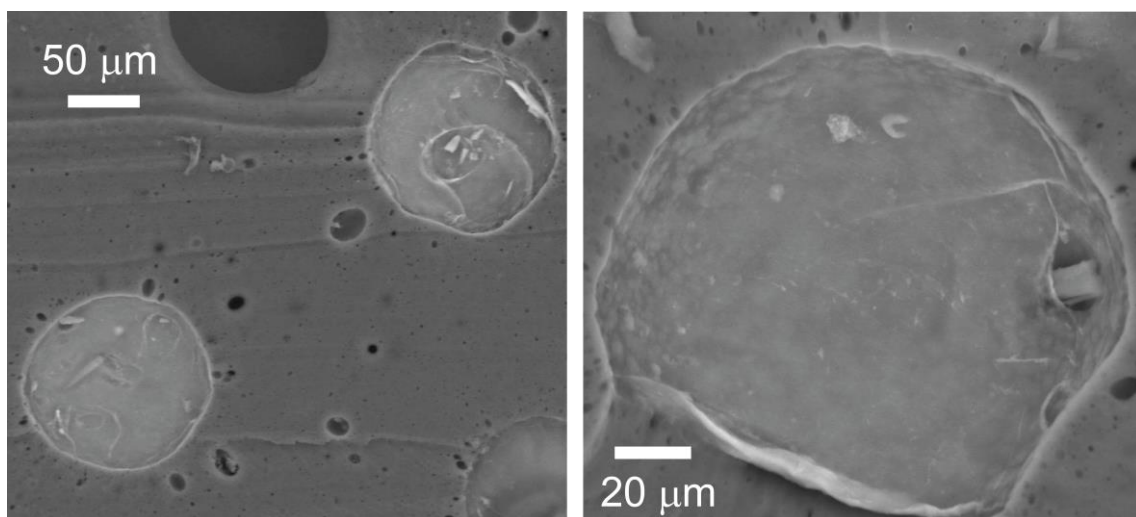**Table S-5.** Details of the hydrogel samples for the UV-Vis measurement.

Figure S-1. Antifouling biocides can be introduced into paint formulation by (a) molecular dispersion, (b) immobilization to a large component, and (c) encapsulation.
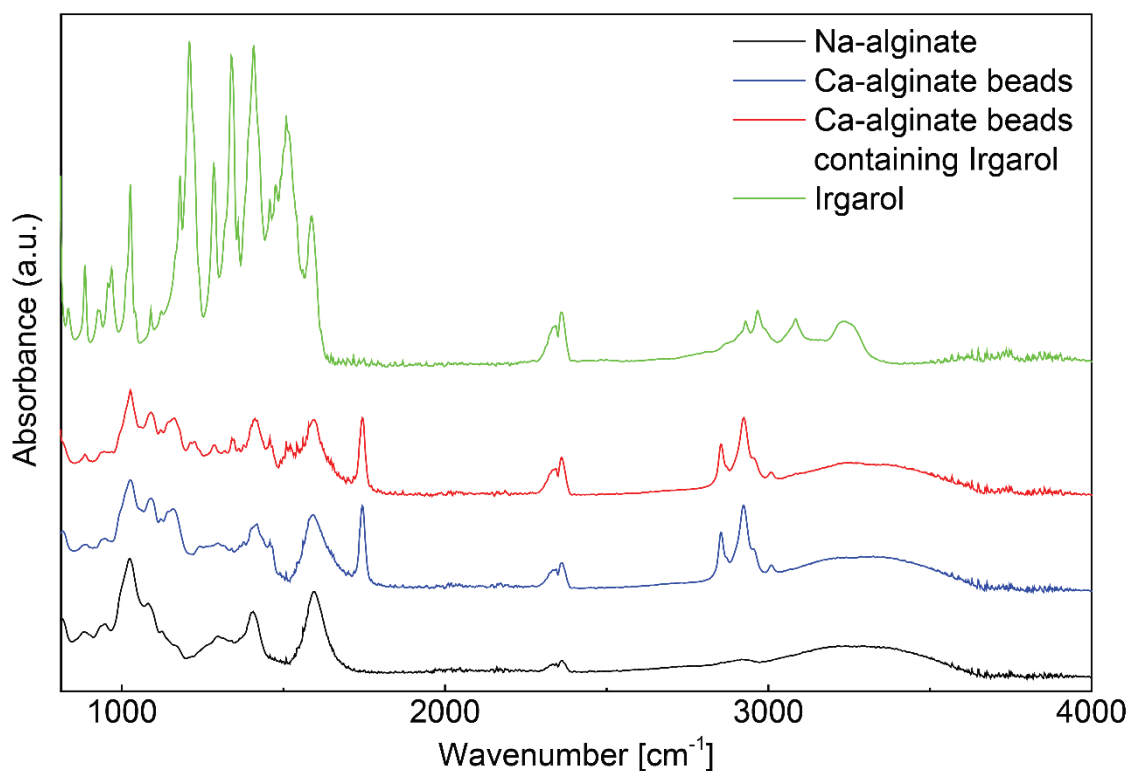
Photosynthesis process

**Figure S-2.** Antifouling mechanism of Irgarol on aquatic plant species.

Figure S-3. Scanning electron microscopy (SEM) images of the cross-section of the Ca-alginate hydrogel particles.

Figure S-4. ATR-FTIR spectra of sodium alginate (Na-alginate) powder, synthesized Ca-alginate particles, Ca-alginate particles containing Irgarol, and Irgarol powder. For the spectra of Ca-alginate particles, compared with the Na-alginate powder, the asymmetric stretching peak of –COO⁻ at 1590 cm^{-1} is gradually replaced by a new absorption peak at 1624 cm^{-1}, which is caused by the interaction of Ca^{2+} with the –COO⁻ groups of Na-alginate [1]. Further, the spectrum of the Ca-alginate beads with Irgarol shows more absorption peaks than the Ca-alginate beads without Irgarol in the wavenumber ranging from 1552 cm^{-1} to 1198 cm^{-1}, suggesting the presence of Irgarol. The absorption peaks at 2925 cm^{-1} and 2854 cm^{-1} of the hydrogel samples were caused by the residual corn oil [2].
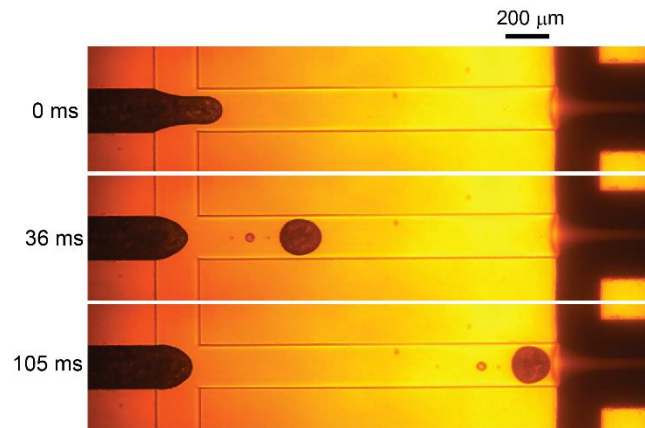
Figure S-5. High speed photomicrographs showing the break-off of a Na-alginate droplet containing both the drug and cellulose fibers. Flow rates of the droplet phase, carrier oil phase, and reactant emulsion stream are 0.1 mL/h, 2.0 mL/h (= 1.0 mL/h × 2) and 20.0 mL/h (= 10.0 mL/h × 2), respectively.
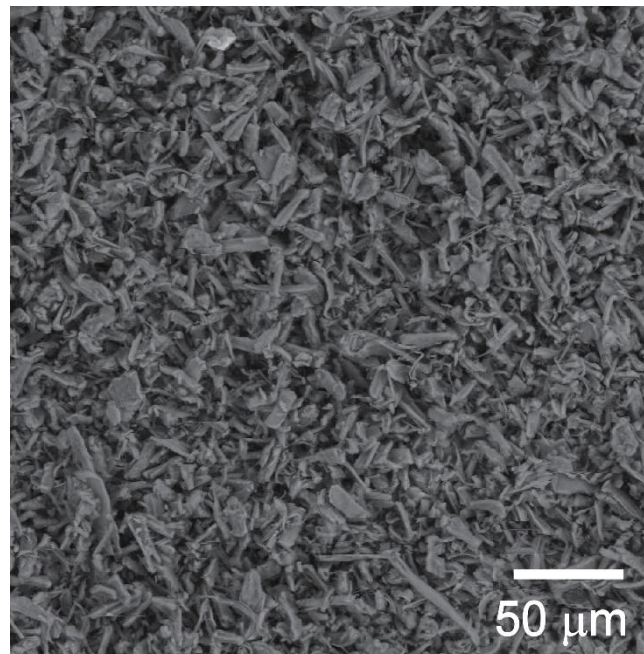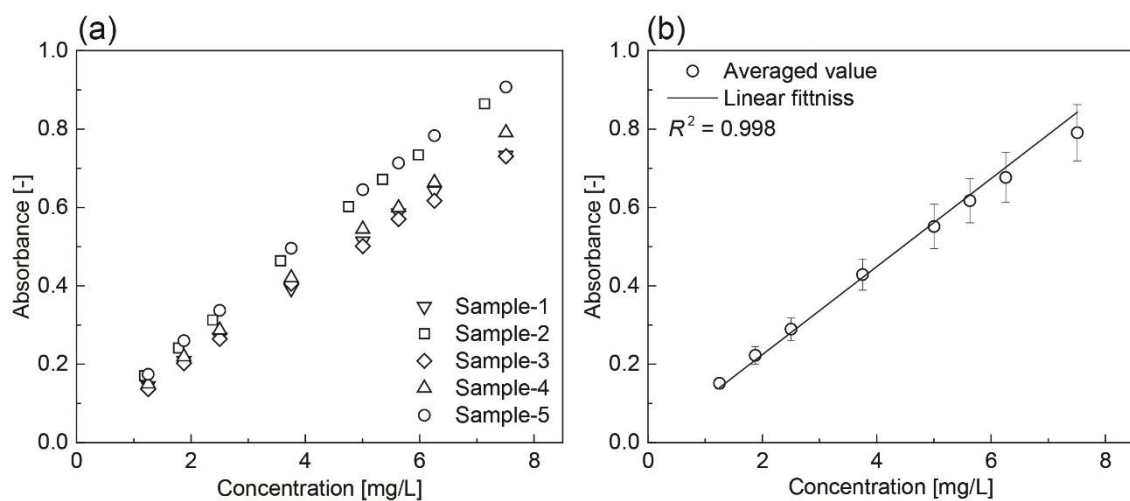

Figure S-6. An SEM image of the cellulose fibers.
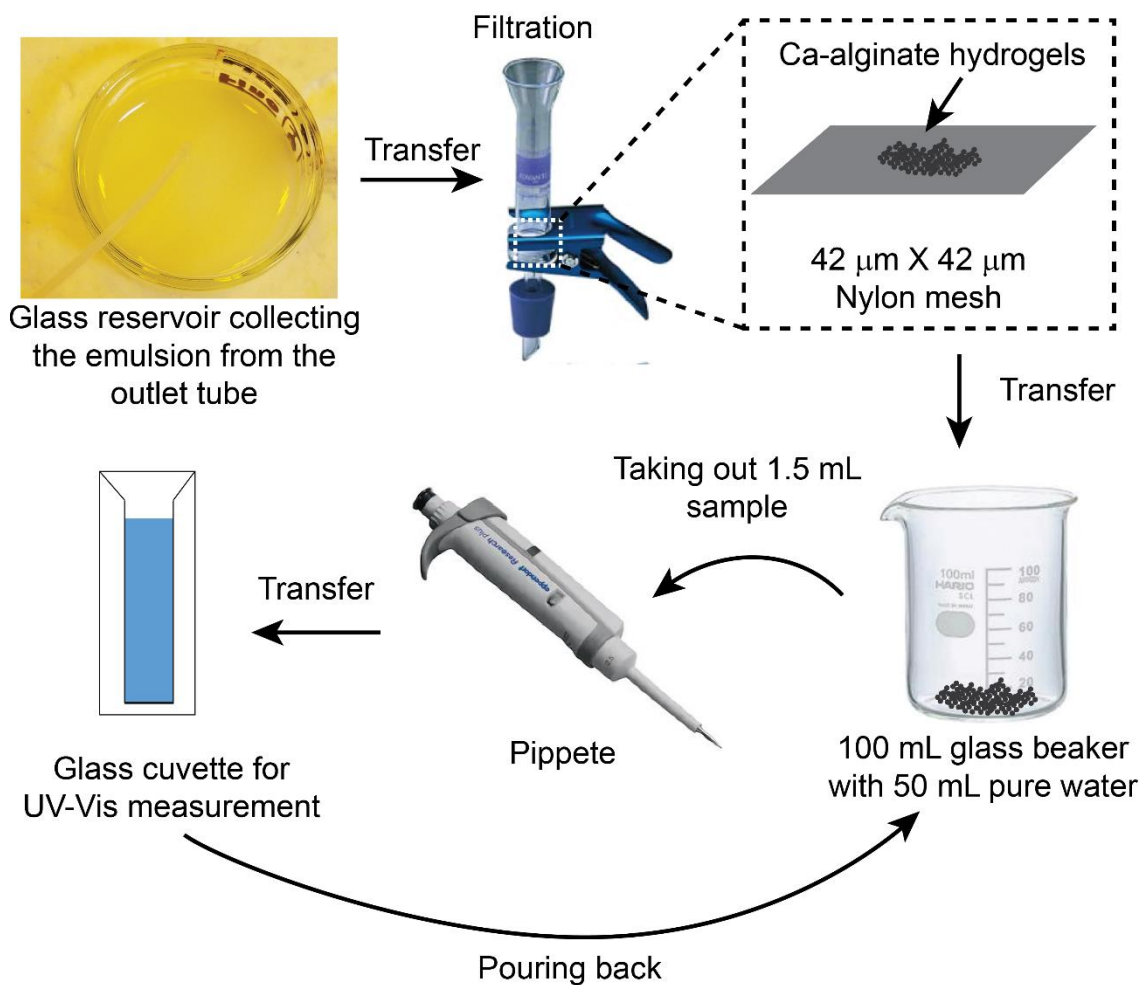
Figure S-7. Schematic illustration of the UV-Vis measurement process.
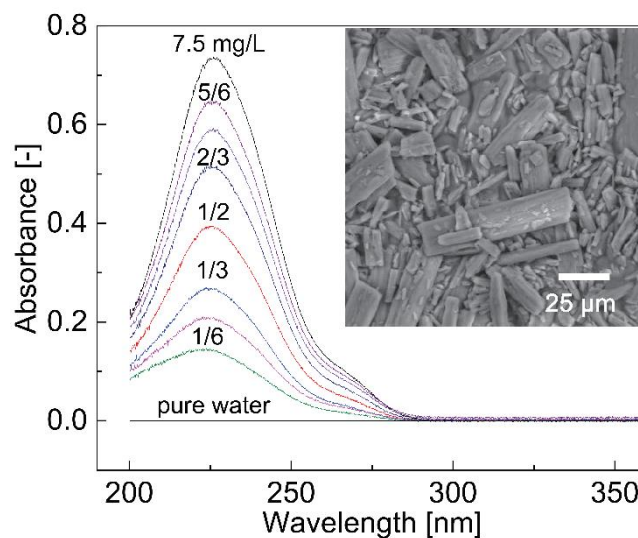
Figure S-8. Measurement of UV-Vis absorbance spectra of Irgarol (Sample 1) at different dilution

ratios. The inset is an SEM image of Irgarol.

Figure S-9. Relationship between the UV-Vis absorbance and the drug concentration. (a) Relationship between the UV-Vis absorbance and the drug concentration of five samples. (b) The average data and linear fitting.
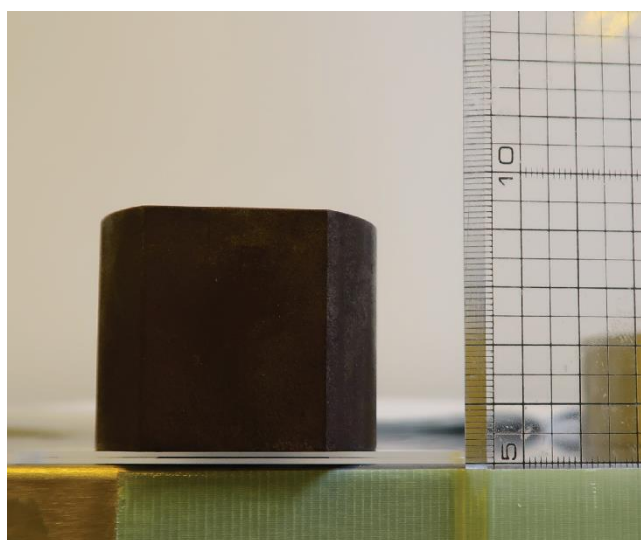
Figure S-10. A photograph from the side showing the particles deformation measurement.

Table S-1. Sizes and size distributions of microcapsules for biocides encapsulation in literature.

Materials	Biocides	Average diameter	Coefficient variation	Reference
PLA (Poly(L-lactide))	Chlorhexidine	1 μm	N.A.	[19]
PLGA and PLGA-PEG	Perfluorooctyl bromide	12–26 μm	N.A.	[20]
Melamine formaldehyde	Aldehydes, alcohols, esters	15 μm	13%	[21]
PMMA	Medetomidine	12 μm	41.6%	[8]
PMMA	Dodecane	2.4 μm	19%	[22]
PMMA	IPBC	N.A.	N.A.	[23]
PMMA	Aurantiol	20–200 μm	N.A.	[24]

Table S-2. Contents of the disperse phase used in the experiment.

	3 wt% Na-alginate solution	Irgarol® 1071	Cellulose fiber	Mixing time (30000 rpm)
Disperse #1	20.0 g	0.1 g	-	3 min
Disperse #2	20.0 g	0.05 g	-	3 min
Disperse #3	20.0 g	0.1 g	1.0 g	5 min

Table S-3. The details of the five samples.

	Water (mL)	Drug weight (mg)	Concentration (mg/L)
Sample 1	399.6	3.0	7.5
Sample 2	399.4	2.9	7.3
Sample 3	399.5	3.0	7.5
Sample 4	399.4	3.0	7.5
Sample 5	399.6	3.0	7.5

Table S-4. Results of the linear fitting.

Intercept		Slope		Statistics
Value	Standard Error	Value	Standard Error	Adj. R-Square
0.02245	0.00363	0.10524	0.00137	0.99841

Table S-5. Details of the hydrogel samples for the UV-Vis measurement.

	The type of used disperse phase	Collection time	Encapsulated amount (m_e)
Type 1	Disperse #1	30 min	0.250 mg
Type 2	Disperse #2	30 min	0.125 mg
Type 3	Disperse #1	60 min	0.500 mg
Type 4	Disperse #2	60 min	0.250 mg
Type 5	Disperse #3	60 min	0.500 mg

References

(1)   Saarai, A.; Kasparkova, V.; Sedlacek, T.; Saha, P. On the development and characterisation of crosslinked sodium alginate/gelatine hydrogels. *J. Mech. Behav. Biomed.* **2013**, *18*, 152–166.

(2)   Setyaningrum, D. L.; Riyanto, S.; Rohman, A. Analysis of corn and soybean oils in red fruit oil using FTIR spectroscopy in combination with partial least square. *Int. Food Res. J.* **2013**, *20*, 1977–1981.